Hydrogenation of 1-Nitroanthraquinone to 1-Aminoanthraquinone Catalyzed by Bimetallic CuPt$_x$ Nanoparticles

Chenchen Yang, Aili Wang, and Hengbo Yin*

Faculty of Chemistry and Chemical Engineering, Jiangsu University, Zhenjiang 212013, China

Bimetallic CuPt$_x$ nanoparticles were prepared in ethanol solution by the wet chemical reduction method using Cu(NO$_3$)$_2$ and H$_2$PtCl$_6$ as starting materials, hydrazine hydrate as a reductant, and polyvinyl pyrrolidone as an organic modifier. The average particle sizes of Cu and Pt nanoparticles were 60 nm and 3 nm, respectively. The small-sized Pt nanoparticles were evenly anchored at the surfaces of large-sized Cu nanoparticles, forming Cu@Pt core–shell structured nanocomposites. In the bimetallic CuPt$_x$ nanoparticles, electron was transferred from platinum to copper species, which increased the selectivity of 1-aminoanthraquinone by suppressing the high hydrogenation activity of metallic platinum. The CuPt$_{0.1}$ bimetallic nanoparticles exhibited higher catalytic activity for the hydrogenation of 1-nitroanthraquinone to 1-aminoanthraquinone than both monometallic Cu and Pt nanoparticles. Over the CuPt$_{0.1}$ catalyst, the selectivity of 1-aminoanthraquinone was 99.3% at the 1-nitroanthraquinone conversion of 98.9%.

Keywords: Bimetallic CuPt$_x$ Nanoparticles, 1-Nitroanthraquinone, Hydrogenation.

1. INTRODUCTION

1-Aminoanthraquinone is an important chemical widely used for the preparation of dyes,[1–3] fluorescers,[4] anticancer medicals,[5] corrosion inhibitors,[6,7] chemical sensors, and biochemicals.[8]

Currently, 1-aminoanthraquinone is commercially produced via the reduction of 1-nitroanthraquinone with sodium sulfite and/or sodium sulfide at 120 °C, accompanied by the formation of sodium sulfate (500 tons of sodium sulfate aqueous solution per ton of 1-aminoanthraquinone). The organic-containing sodium sulfate aqueous solution caused a severe pollution problem. To avoid the pollution, researchers have been seeking alternative catalytic reduction of 1-nitroanthraquinone with hydrogen over various catalysts, such as Pd/C,[9] Pd/Al$_2$O$_3$,[10] and Ni[9,11] catalysts in China, giving the 1-aminoanthraquinone yield of ca. 90%. Pd-based catalysts exhibited good catalytic activity for the hydrogenation of 1-nitroanthraquinone to 1-aminoanthraquinone. How to increase the selectivity of 1-aminoanthraquinone and decrease catalyst cost is still worthy of investigation.

Recently, bimetallic nanoparticles have attracted researcher's attention because they exhibited better

catalytic performances for chemical reactions than monometallic nanoparticles. Bimetallic AuPd nanoparticles exhibited excellent catalytic activity for the selective oxidation of methane to methanol with a high selectivity of 92% at 50 °C in an aqueous solution.[12] Au$_3$Cu nanoparticles exhibited higher catalytic activity for the electrochemical reduction of CO$_2$ than both monometallic Au and Cu nanoparticles.[13] Bimetallic PdPt nanoparticles were two and a half times more active in the oxygen reduction reaction than Pt/C catalyst and five times more active than commercial Pt black catalyst.[14] The interaction between two metals in bimetallic nanoparticles plays an important role in the catalytic reactions.

In our present work, we found that bimetallic CuPt nanoparticles could effectively catalyze the hydrogenation of 1-nitroanthraquinone with H$_2$ to 1-aminoanthraquinone. The structural effect of the bimetallic CuPt nanoparticles on the reduction reaction was analyzed and discussed.

2. EXPERIMENTAL DETAILS

2.1. Materials

Hexachloroplatinic acid hexahydrate (H$_2$PtCl$_6$ · 6H$_2$O, >98%), copper nitrate trihydrate (Cu(NO$_3$)$_2$ · 3H$_2$O, >99%), hydrazine hydrate (N$_2$H$_4$ · H$_2$O, 85%), polyvinyl

---

*Author to whom correspondence should be addressed.

pyrrolidone (PVP, K30), sodium hydroxide (96%), anhydrous ethanol (>99.7%), 1-nitroanthraquinone (95%), 1-aminoanthraquinone (97%), and N,N-dimethylformamide (DMF, >99.5%) were of analytical reagent grade and were purchased from Sinopharm Group Co. Ltd.

2.2. Preparation of Bimetallic CuPt$_x$ Nanoparticles

Bimetallic CuPt$_x$ nanoparticles were prepared by the wet chemical reduction method using hydrazine hydrate as a reductant and PVP as an organic modifier. A typical preparation procedure was described as follows. Firstly, given amount of $H_2PtCl_6 \cdot 6H_2O$ (0.0386 mol L^{-1}) ethanol solution and 26 mL of organic modifier (10 wt% of $Cu(NO_3)_2 \cdot 3H_2O$) ethanol solution were mixed. Sixty milliliters of copper nitrate (0.1667 mol L^{-1}) ethanol solution was added into the above solution under stirring. After the mixed solution was heated to 60 °C, the pH value of the solution was adjusted to 10 with a NaOH (1.0 mol L^{-1}) ethanol solution. And then, 20 mL of hydrazine (7.5 mol L^{-1}) ethanol solution was added dropwise at a rate of 1.2 mL min^{-1}. The reduction reaction lasted for 4 h with gentle stirring. The color of the reaction solution became black, indicating that the Cu^{2+} and Pt^{4+} were reduced to metallic Cu^0 and Pt^0. The CuPt$_x$ nanoparticles were cooled to room temperature, centrifugated at 9000 rpm, and washed with anhydrous ethanol for 6 times. The resultant bimetallic CuPt$_x$ nanoparticles were kept in anhydrous ethanol. The atomic ratio of Pt to Cu was changed by the volume of $H_2PtCl_6 \cdot 6H_2O$ ethanol solution.

For the purpose of comparison, monometallic Cu nanoparticles and monometallic Pt nanoparticles were also prepared according to the above-mentioned procedures.

2.3. Characterization

The crystal phases of the as-prepared Cu, Pt, and CuPt$_x$ nanoparticle samples were determined by X-ray powder diffraction (XRD). The XRD spectra of the samples were recorded on a diffractometer (D8 super speed Bruke-AEX Company, Germany) using Cu Kα radiation ($\lambda =$ 1.54056 Å) at room temperature, scanning from 30° to 85° (2θ).

Transmission electron microscopy (TEM) images are obtained using a microscope (JEM-2100) operated at an acceleration voltage of 200 kV to characterize the morphologies and particle sizes of the resultant nanoparticles. TEM specimens were prepared by dropping ethanol suspension of nanoparticle sample onto a copper grid. The data used for calculating the particle sizes for each sample were measured from the TEM images by counting at least 100 individual particles. The average particle size of the metallic nanoparticles was calculated by a weighted average method based on the size of every individual counted particle.

The EDX and EDS elemental mapping images of the bimetallic samples were recorded on a scanning electron microscope (JSM-6010 PLUS/LA), operating at an accelerating voltage of 15 kV.

The X-ray photoelectron spectra (XPS) of the samples were performed on a Thermo ESCALAB 250Xi X-ray photoelectron spectrometer with monochrome Al Kα ($h\nu =$ 1486.6 eV) as X-ray excitation source. The XPS of the samples were calibrated by using Cls of 284.6 eV as the internal standard.

Inductively coupled plasma spectrometer (ICP) analyses were performed using a VISTA–MPX instrument to verify the atomic ratio of Cu and Pt in the bimetallic CuPt$_x$ samples.

2.4. Evaluation of Catalytic Performance

Catalytic hydrogenation of 1-nitroanthraquinone with H_2 was performed in a 500 mL stainless steel autoclave and stirred with a magnetic driven stirrer. The autoclave was charged with 3 g of 1-nitroanthraquinone in 150 mL of DMF solution and appointed amount of CuPt$_x$ nanoparticles. The autoclave was purged with N_2 for 10 min to replace air inside. And then, pure H_2 was pressurized into the autoclave and the reaction solution was heated to specified reaction temperatures. When the reaction temperature reached the specified value, the stirring rate was increased to 400 rpm. After reacting for a period of time, the reaction was quenched by running cooling water through a cooling coil in the autoclave. The products were analyzed using high performance liquid chromatography (HPLC). A reverse-phase column (Innoval ASB C18, 5 mm, 4.6 mm × 250 mm) and a UV detector ($\lambda =$ 254 nm) were used for analysis at 30 °C. A mixture of water and methanol of chromatographic grade (v/v, 20/80) was used as a mobile phase at a flow rate of 1.0 mL min^{-1}. The concentrations of the products and 1-nitroanthraquinone were analyzed by the external standard method.

3. RESULTS AND DISCUSSION

3.1. Chemical Structure and Composition Analyses by XRD and ICP

The XRD patterns showed that the XRD peaks of the monometallic copper sample appeared at (2θ) 43.3, 50.4, and 74.0°, respectively, which were consistent with the (111), (200), and (220) crystal planes of face-centered cubic metallic copper (JCPDS 04-0836) (Fig. 1). The XRD peaks of the monometallic platinum sample appeared at 39.7, 46.3, 67.5, and 81.2°, corresponding to the (111), (200), (220), and (311) crystal planes of metallic platinum (JCPDS 04-0802), respectively.

For the bimetallic CuPt$_x$ samples, the XRD peaks of metallic copper were detected. However, no XRD peaks of metallic platinum were found. It is possibly for the reason that the amount of platinum was too small to be detected by XRD technique and/or that platinum particles with small sizes were well dispersed in the samples. Interestingly, it was found that the XRD peaks of the metallic
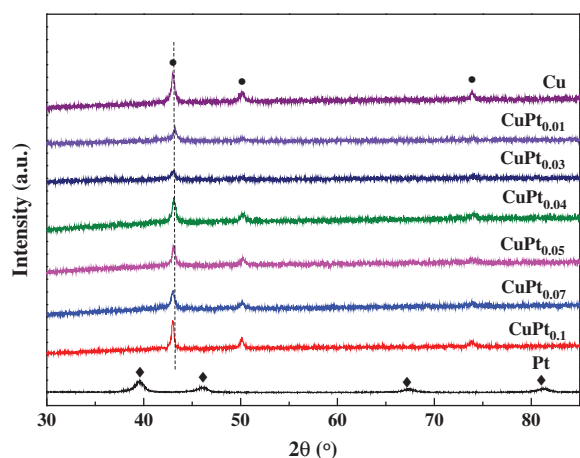
Figure 1. The XRD patterns of the bimetallic CuPt$_x$, monometallic Cu, and monometallic Pt nanoparticles. ●, metallic Cu; ◆, metallic Pt.

copper in the bimetallic CuPt$_x$ samples shifted to lower 2θ values as compared with those of monometallic Cu sample. The shift extents of XRD peaks increased with the increase in platinum content. When the atomic ratio of Pt to Cu was increased to 0.1:1, the XRD peaks of (111), (200), and (220) crystal planes of metallic copper shifted, respectively, by 0.24, 0.20, and 0.08° as compared with those of monometallic copper sample. The results indicated that there was an interaction between metallic copper and metallic platinum in the bimetallic CuPt$_x$ nanoparticles.

The crystallite sizes of Cu(111) in the samples were calculated according to Scherrer's equation and the data are listed in Table I. The crystallite sizes of Cu(111) in both monometallic Cu and bimetallic CuPt$_x$ samples were around 20 nm, indicating that metallic copper nanoparticles were present in the as-prepared samples. On the other hand, the ICP analysis showed that the compositions of the CuPt$_x$ samples were close to those in their starting materials (Table I). Copper and platinum ions could be effectively reduced to their metallic states under our present experimental conditions.

3.2. Morphology, Particle Size, and EDS Elemental Mapping Analyses

The TEM images of the monometallic Cu and Pt samples show that the monometallic copper sample was composed of Cu nanoparticles with the average particle size of 60 nm and the monometallic platinum sample was composed of extreme fine Pt nanoparticles with the average particle size of 3 nm (Figs. 2(a, b)). For the CuPt$_x$ samples, they were composed of both Pt and Cu nanoparticles (Figs. 2(c–h)). The average particle sizes of the Cu and Pt nanoparticles were similar to those of monometallic Cu and Pt nanoparticles, respectively. The size distributions of the Pt nanoparticles in the CuPt$_x$ samples were in a narrower range of 1–7 nm (Table I). The TEM images clearly show that the Pt nanoparticles were well coated on the surfaces of Cu nanoparticles. The coating extent increased with the increase in the Pt/Cu atomic ratios.

Additionally, the EDS elemental mapping images show the uniform distributions of Cu and Pt atoms throughout the selected samples, implying that the metallic Pt nanoparticles were well dispersed in the bimetallic CuPt$_x$ samples (Fig. 3). The EDX analysis showed that the atomic ratios of Pt to Cu increased with the increase in the Pt contents (Table II). And these values of the Pt/Cu ratios were larger than those analyzed by ICP analysis. Combined both EDX and EDS elemental mapping analyses, it is reasonable to conclude that Pt nanoparticles could be well coated on the surfaces of Cu nanoparticles.

3.3. Surface Chemical State Analysis by XPS

The surface chemical structures of the monometallic Cu, monometallic Pt, and representative bimetallic CuPt$_x$ samples were analyzed by XPS technique (Fig. 4).

Table I. The physicochemical properties of monometallic Cu, monometallic Pt, and bimetallic CuPt$_x$ nanoparticles and their catalytic activities in the catalytic hydrogenation of 1-nitroanthraquinone to 1-amioanthraquinone.

Catalysts	Atomic ratios of Cu/Pt[a]	Crystallite sizes of metallic Cu(111)[b] (nm)	Average particle sizes of Pt[c] (nm)	Conversions of 1-nitroanthraquinon[d] (%)	Selectivities (%)		Reaction rates[e] (mol$_{1\text{-NAQ}}$ mol$_{Pt}^{-1}$ h^{-1})
					1-amino-anthraquinone	1-amino-hydroquinone	
Cu	–	19.2	60.0, (21–116) (Cu)	3.3	100	0	–
CuPt$_{0.01}$	1:0.01	17.5	3.3, (2–5)	5.9	99.8	0.2	6.4
CuPt$_{0.03}$	1:0.03	19.7	3.2, (1–5)	8.4	99.6	0.4	3.2
CuPt$_{0.04}$	1:0.04	20.1	3.0, (1–6)	17.4	99.7	0.3	5.1
CuPt$_{0.05}$	1:0.05	19.8	3.6, (2–6)	36.9	99.6	0.4	8.9
CuPt$_{0.07}$	1:0.07	19.5	3.0, (1–5)	66.7	99.4	0.6	12.1
CuPt$_{0.1}$	1:0.11	24.0	2.9, (1–7)	98.9	99.3	0.7	12.7
Pt[f]	–	1.5 (Pt)	3.0, (1–6)	98.0	78.5	21.5	101
Pt[g]	–	1.5 (Pt)	3.0, (1–6)	100	61.9	38.1	–

Notes: [a]The atomic ratios of Cu/Pt were analyzed by using ICP. [b]The crystallite sizes of metallic Cu(111) and Pt(111) were calculated according to the Scherrer's equation. [c]The average particle sizes and size distributions of metallic Cu and Pt were determined according to their TEM images. [d]The reaction conditions: catalyst, 0.18 g; 3 g of 1-nitroanthraquinone was dissolved in 150 *N*,*N*-dimethylformamide; 140 °C for 4 h; H$_2$ pressure, 0.5 MPa. [e]Reaction rate = reacted 1-nitroanthraquinone (mol)/reaction time/platinum amount (mol) in catalyst. [f,g]The catalyst loading of monometallic Pt was the same as that in CuPt$_{0.1}$ catalyst. The reaction times were 0.5 and 4 h, respectively.
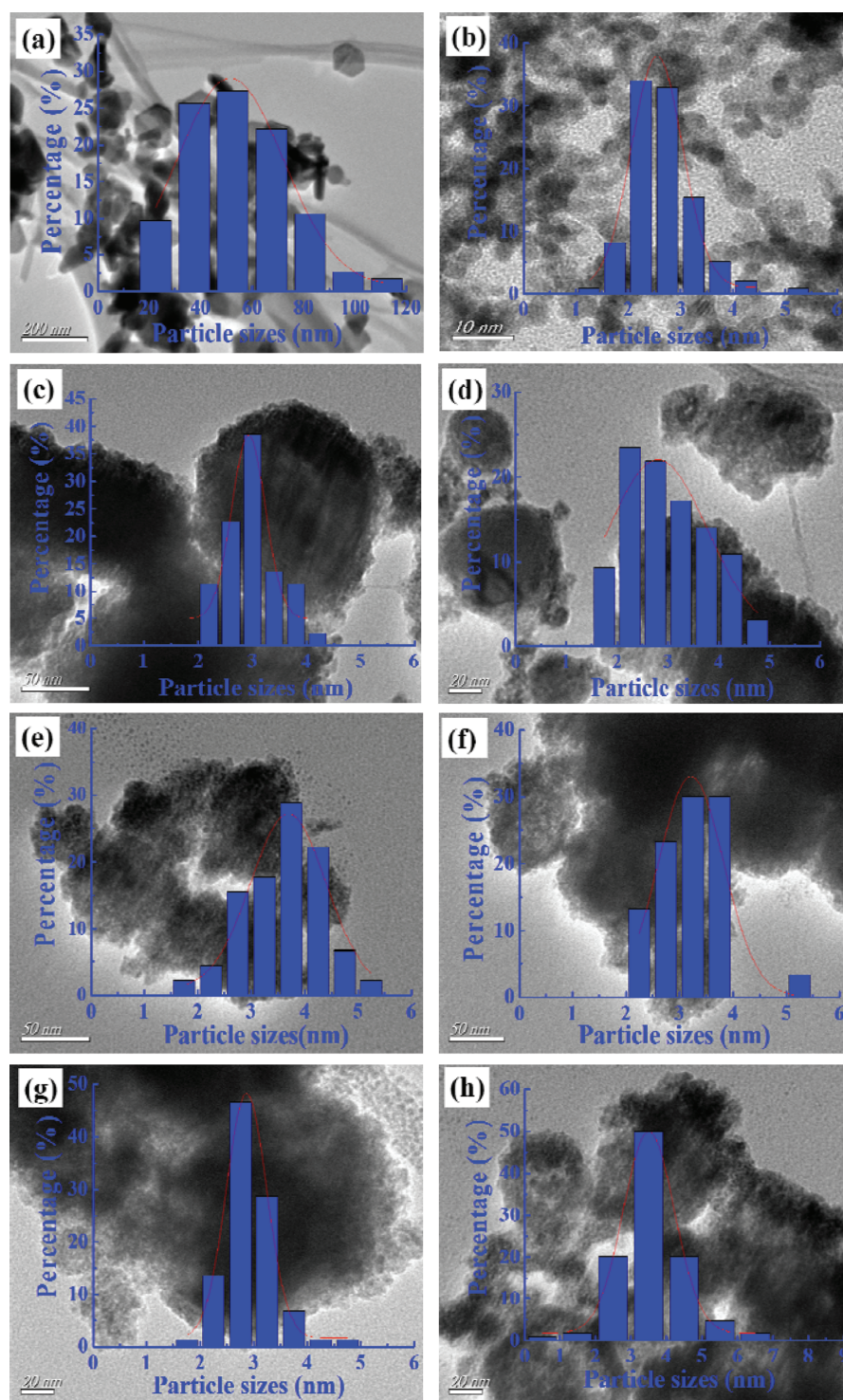
Figure 2. TEM images of monometallic Cu, monometallic Pt, and bimetallic CuPt$_x$ samples and particle size distributions of Cu nanoparticles in monometallic Cu sample and Pt nanoparticles in bimetallic CuPt$_x$ samples. (a) Monometallic Cu sample; (b) monometallic Pt sample; and (c–h) bimetallic CuPt$_{0.01}$, CuPt$_{0.03}$, CuPt$_{0.04}$, CuPt$_{0.05}$, CuPt$_{0.07}$, and CuPt$_{0.1}$ samples.

The binding energies of Cu$2p_{3/2}$ and Cu$2p_{1/2}$ of the monometallic Cu, CuPt$_{0.05}$, and CuPt$_{0.1}$ samples were 932.5, 952.3; 932.4, 952.2; 932.3, 952.1 eV, respectively (Fig. 4(a)). The chemical states of copper component in these samples were Cu$^+$ and/or Cu^0 because no satellite peak at 942.5 eV was found.[15] The binding energy of Cu$2p$ slightly shifted to a lower value with the increase in Pt content.
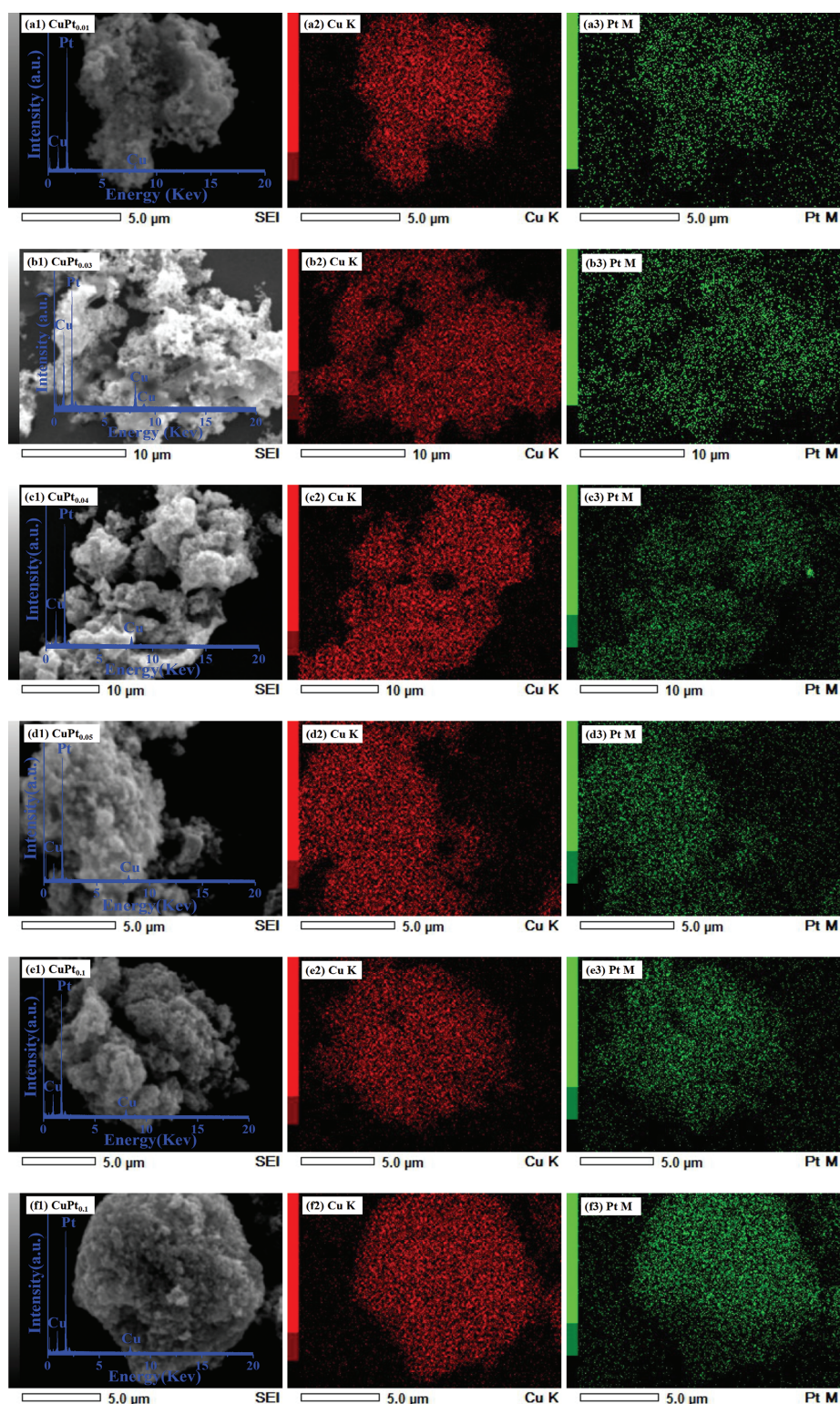
Figure 3. EDX patterns and EDS elemental mapping images of bimetallic CuPt$_x$ samples. (a–f) bimetallic CuPt$_{0.01}$, CuPt$_{0.03}$, CuPt$_{0.04}$, CuPt$_{0.05}$, CuPt$_{0.07}$, and CuPt$_{0.1}$ samples.

To ascertain the chemical states of the surface copper species, the XAES peaks were deconvoluted (Fig. 4(b)). Using Gaussian-Lorentzian bands with the peak positions at ca. 915 and 918 eV for Cu$^+$ and Cu^0,[16, 17] the XAES peaks were deconvoluted into two symmetrical peaks. According to the deconvolution results, the surface copper species of the monometallic Cu, CuPt$_{0.05}$, and CuPt$_{0.1}$ samples were composed of Cu$^+$ and metallic Cu^0 components.

Table II. Cu/Pt atomic ratios on the surfaces of bimetallic CuPt$_x$ nanoparticles analyzed by EDX.

Samples	CuPt$_{0.01}$	CuPt$_{0.03}$	CuPt$_{0.04}$	CuPt$_{0.05}$	CuPt$_{0.07}$	CuPt$_{0.1}$
Cu/Pt atomic ratios	1:0.02	1:0.03	1:0.05	1:0.06	1:0.10	1:0.11

Their Cu^+/Cu^0 ratios were 2.7:1, 4.6:1, and 8:1. The ratios of surface Cu^+ to Cu^0 were increased with the Pt content. The high oxidation state at the Cu surface was probably caused by the oxidation of metallic Cu^0 when the CuPt$_x$ samples were exposed in air during the sample characterization. The presence of Pt probably promoted the oxidation of metallic Cu^0.

The binding energies of $Pt4f_{7/2}$ and $Pt4f_{5/2}$ of the monometallic Pt, CuPt$_{0.1}$, and CuPt$_{0.05}$ samples were 71.2, 74.6; 71.3, 74.8; 71.8, 75.2 eV, respectively (Fig. 4(c)). The chemical state of platinum component in these samples was metallic Pt^0.[18–22] The binding energies of $Pt4f$ of the CuPt$_x$ samples shifted to higher values as compared with the monometallic Pt. The XPS analysis revealed that there was an interaction between platinum and copper components in the CuPt$_x$ samples. According to the shift of $Cu2p$ and $Pt4f$, it could be suggested that electron was transferred from platinum to copper species.

3.4. Catalytic Hydrogenation of 1-Nitroanthraquinone

The reaction processes for the catalytic hydrogenation of 1-nitroanthraquinone are shown in Scheme 1, in which 1-aminoanthraquinone and 1-aminohydroquinone are stable products. 1-Nitrosoanthraquinone and 1-hydroxy-aminoanthraquinone as the intermediates could be rapidly and subsequently hydrogenated to 1-aminoanthraquinone. 1-Aminoanthraquinone could be further hydrogenated to 1-aminohydroquinone.

The conversion of 1-nitroanthraquinone was only 3.3% over the monometallic Cu catalyst at 140 °C for 4 h (Table I). With increasing the Pt content in the bimetallic CuPt$_x$ catalysts, the conversion increased to 98.9% at a Pt/Cu atomic ratio of 0.1:1. The selectivity of 1-aminoanthraquinone was above 99% over the monometallic Cu and all CuPt$_x$ catalysts. Interestingly, when the monometallic Pt nanoparticles were used as the catalysts with the Pt content equivalent to that in CuPt$_{0.1}$ at 140 °C for 0.5 h, the selectivity of 1-aminoanthraquinone was 78.5% at the conversion of 1-nitroanthraquinone of 98%. 1-Aminohydroquinone with the selectivity of 21.5% was formed as the by-product via hydrogenation of resultant 1-aminoanthraquinone. Upon increasing the reaction time to 4 h, the conversion of 1-nitroanthraquinone reached 100%, the selectivity of 1-aminoanthraquinone decreased to 61.9% meanwhile the selectivity of 1-aminohydroquinone increased to 38.1%. Over the monometallic Pt nanoparticles, the desired 1-aminoanthraquinone could be further hydrogenated to produce 1-aminohydroquinone as compared with the bimetallic CuPt$_x$ nanoparticles.
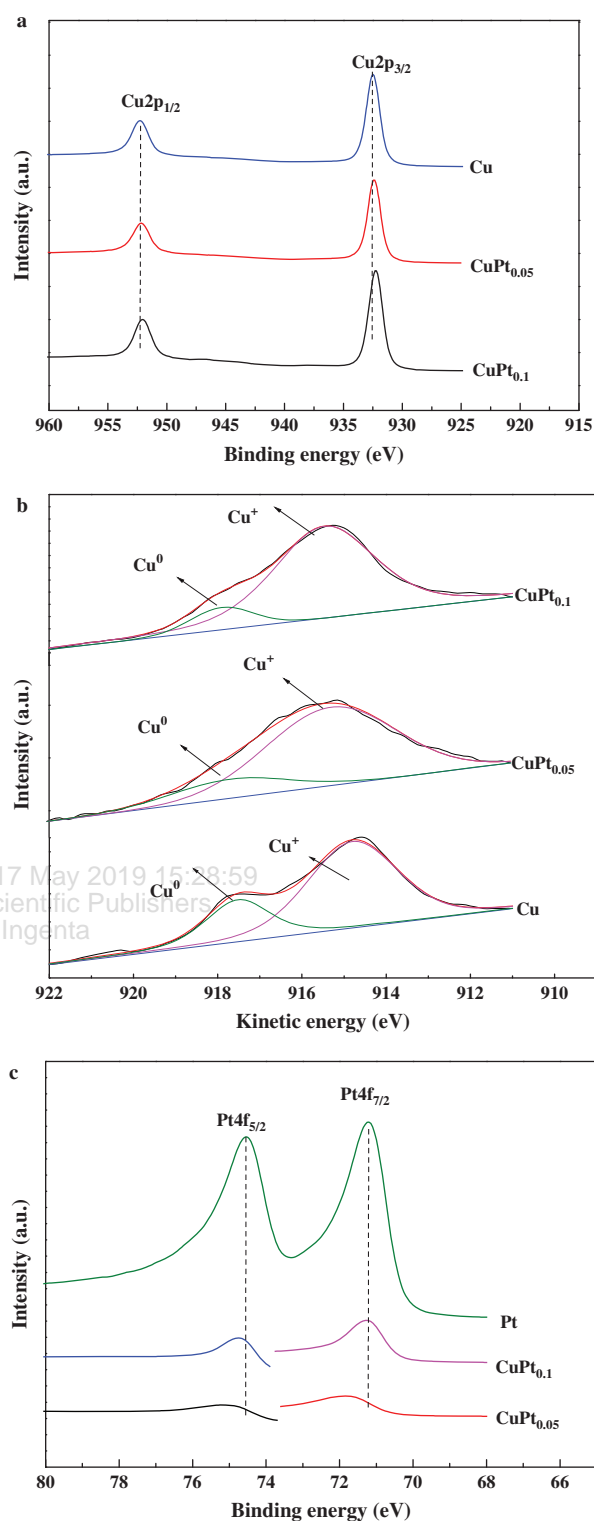
Figure 4. XPS of Cu $2p$ and Pt $4f$ of the representative monometallic Cu, monometallic Pt, and bimetallic CuPt$_x$ catalysts. (a) Cu $2p$; (b) deconvolution of Cu XAES peaks; (c) Pt $4f$.

When the bimetallic CuPt$_x$ catalysts with the Pt/Cu atomic ratios of 0.05:1–0.1:1 were used as the catalysts, their reaction rates ranged from 8.9 to 12.7 mol$_{1\text{-NAQ}}$ mol$_{Pt}^{-1}$ h^{-1}, which were much less than that of the
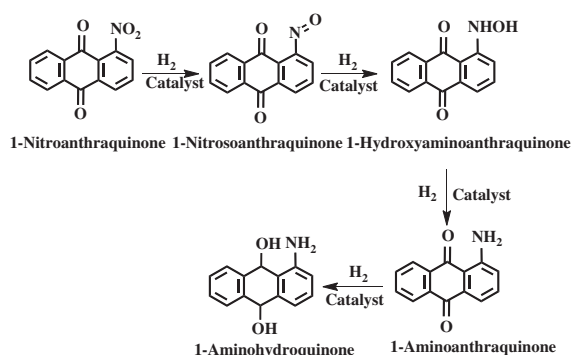
Scheme 1. Catalytic hydrogenation processes of 1-nitroanthraquinone.
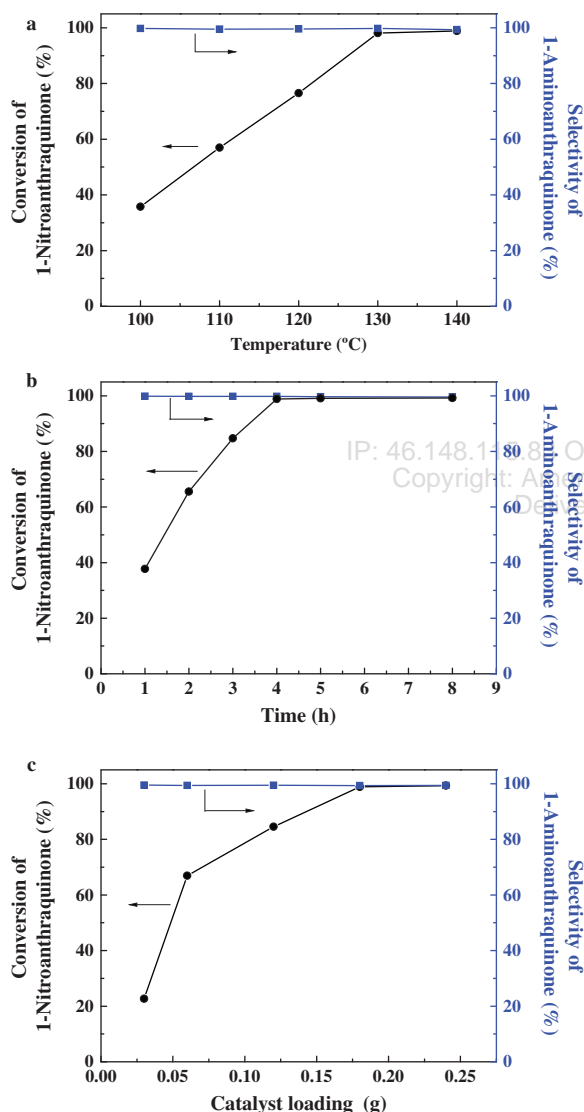
Figure 5. Effect of reaction parameters on the catalytic hydrogenation of 1-nitroanthraquinone (1-NAQ) to 1-aminoanthraquinone (1-AAQ) over CuPt$_{0.1}$ catalyst. Reaction conditions: (a) Catalyst, 0.18 g; 3 g of 1-NAQ dissolved in 150 N,N-dimethylformamide; reaction time for 4 h; H$_2$ pressure, 0.5 MPa. (b) Catalyst, 0.18 g; 3 g of 1-NAQ dissolved in 150 N,N-dimethylformamide; 140 °C; H$_2$ pressure, 0.5 MPa. (c) 3 g of 1-NAQ dissolved in 150 N,N-dimethylformamide; 140 °C for 4 h; H$_2$ pressure, 0.5 MPa.

monometallic Pt catalyst. The results revealed that the interaction between Pt and Cu in bimetallic CuPt$_x$ nanoparticles favored the catalytic hydrogenation 1-nitroanthraquinone to 1-aminoanthraquinone, suppressing the nonselective and high hydrogenation activity of the monometallic Pt nanoparticles.

3.5. Effect of Reaction Temperature, Reaction Time, and Catalyst Loading

The bimetallic CuPt$_{0.1}$ nanoparticles were used as the model catalysts to investigate the effect of reaction parameters, such as reaction temperature, reaction time, and catalyst loading, on the hydrogenation reaction (Fig. 5). Upon increasing the reaction temperature to 130 °C, the conversion of 1-nitroanthraquinone increased to 98%. The selectivity of 1-aminoanthraquinone was above 99% at different reaction temperatures (Fig. 5(a)). With prolonging the reaction time to 4 h at 140 °C, the conversion of 1-nitroanthraquinone reached 98.9% (Fig. 5(b)). Increasing catalyst loading favored the conversion of 1-nitroanthraquinone to 1-aminoanthraquinone (Fig. 5(c)). The results showed that bimetallic CuPt$_{0.1}$ nanoparticles exhibited excellent selectivity for the hydrogenation of 1-nitroanthraquinone to 1-aminoanthraquinone.

4. CONCLUSIONS

Bimetallic CuPt$_x$ nanoparticles were prepared by the wet chemical reduction method. The small-sized Pt nanoparticles were well dispersed on the surfaces of large-sized Cu nanoparticles. There was an interaction between Pt nanoparticle and Cu nanoparticle in the bimetallic CuPt$_x$ nanoparticles. The bimetallic CuPt$_{0.1}$ nanoparticles exhibited high catalytic activity for the selective hydrogenation of 1-nitroanthraquinone to 1-aminoanthraquinone under mild reaction temperature. The bimetallic CuPt$_{0.1}$ nanoparticles may have potential application for the hydrogenation reaction.

References and Notes

1. D. Thetford and A. P. Chorlton, *Dyes Pigments* 61, 49 (**2004**).
2. S. M. Burkinshaw and Y.-A. Son, *Dyes Pigments* 87, 132 (**2010**).
3. Y. Chao, Y. Chung, C. Lai, S. Liao, and J. Chin, *Dyes Pigments* 40, 59 (**1998**).
4. M. Shamsipur, M. J. Chaichi, A. R. Karami, and H. Sharghi, *J. Photoch. Photobio. A* 174, 23 (**2005**).
5. H.-S. Huang, C.-L. Chou, C.-L. Guo, C.-L. Yuan, Y.-C. Lu, F.-Y. Shieh, and J.-J. Lin, *Bioorgan. Med. Chem.* 13, 1435 (**2005**).

6. N. Muthukumar, A. Ilangovan, S. Maruthamuthu, and N. Palaniswamy, *Electrochim. Acta* 52, 7183 (**2007**).

7. N. Muthukumar, A. Ilangovan, S. Maruthamuthu, N. Palaniswamy, and A. Kimura, *Mater. Chem. Phys.* 115, 444 (**2009**).

8. Y. Baqi and C. E. Müller, *Tetrahedron Lett.* 53, 6739 (**2012**).

9. C. Wang, *Chemical Intermediate* 1, 21 (**2004**).

10. H. Zhang, H. B. Sun, and M. Huang, *Advances in Fine Petrochemicals* 15, 40 (**2014**).

11. D. Zheng, C. Wu, B. Yan, and W. Li, *Fine and Specialty Chemicals* 25, 47 (**2017**).

12. N. Agarwal, S. J. Freakley, R. U. McVicker, S. M. Althahban, N. Dimitratos, Q. He, D. J. Morgan, R. L. Jenkins, D. J. Willock, S. H. Taylor, C. J. Kiely, and G. J. Hutchings, *Science* 358, 223 (**2017**).

13. D. Kim, J. Resasco, Y. Yu, A. M. Asiri, and P. Yang, *Nat. Commun.* 5, 4948 (**2014**).

14. B. Lim, M. Jiang, P. H. C. Camargo, E. C. Cho, J. Tao, X. Lu, Y. Zhu, and Y. Xia, *Science* 324, 1302 (**2009**).

15. D. Zhang, H. Yin, C. Ge, J. Xue, T. Jiang, L. Yu, and Y. Shen, *J. Ind. Eng. Chem.* 15, 537 (**2009**).

16. H. Lin, X. Zheng, Z. He, J. Zheng, X. Duan, and Y. Yuan, *Appl. Catal. A-Gen.* 445–446, 287 (**2012**).

17. L. Chen, P. Guo, M. Qiao, S. Yan, H. Li, W. Shen, H. Xua, and K. Fan, *J. Catal.* 257, 172 (**2008**).

18. J. Feng, L. He, R. Fang, Q. Wang, J. Yuan, and A. Wang, *J. Power Sources* 330, 140 (**2016**).

19. P. J. Dietrich, R. J. Lobo-Lapidus, T. Wu, A. Sumer, M. C. Akatay, B. R. Fingland, N. Guo, J. A. Dumesic, C. L. Marshall, E. Stach, J. Jellinek, W. N. Delgass, F. H. Ribeiro, and J. T. Miller, *Top. Catal.* 55, 53 (**2012**).

20. R. Peng, S. Li, X. Sun, Q. Ren, L. Chen, M. Fu, J. Wu, and D. Ye, *Appl. Catal. B-Environ.* 220, 46 (**2018**).

21. J. Zhao, H. Matsune, S. Takenaka, and M. Kishida, *Chem. Eng. J.* 308, 963 (**2017**).

22. X. Zhang, Q. Li, M. Xiao, and Y. Liu, *Appl. Catal. A-Gen.* 480, 50 (**2014**).